Sensitivity analysis of a zeolite energy storage model: Impact of parameters on heat storage density and discharge power density

Frédéric Kuznik, Damien Gondre, Kévyn Johannes, Christian Obrecht, Damien David

Sensitivity analysis of a zeolite energy storage model: impact of parameters on heat storage density and discharge power density

Frédéric KUZNIK[a,*], Damien GONDRE[a], Kévyn JOHANNES[b], Christian OBRECHT[a], Damien DAVID[b]

[a] *Université de Lyon, INSA–Lyon, CETHIL UMR5008 F–69621, Villeurbanne, France*
[b] *Université de Lyon, Université Lyon 1, CETHIL UMR5008, F-69622,Villeurbanne, France*

Abstract

Physisorption heat storage in buildings can be a key technology for the more effective use of heating energy. However, a better understanding of key factors influencing the design and control of such systems is necessary. This paper presents the sensitivity analysis of the modeling parameters in the case of an open zeolite 13X / moist air heat storage system for building applications. The quantities of interest are the heat storage density and the discharge power density of the system. At the beginning, the whole analysis space is composed of 21 physical properties and 7 operating conditions and geometrical properties. After a first threshold selection, analysis of variance is carried on the remaining parameters, with a full factorial design of experiments to perform a complete sensitivity analysis of the model. The results show that only 3 thermophysical properties, i.e. the heat of adsorption, the water vapor molar mass and the adsorption equilibrium, and 3 operating conditions and system geometry parameters, i.e. the inlet relative humidity, the bed length and the inlet fluid flow rate, drive the outlet power density

and heat storage density. The way those 6 parameters influence the outputs is also discussed and quantitatively assessed.

Keywords: Physisorption; Heat storage; Numerical modeling; Sensitivity analysis; Optimization; Control

LIST OF SYMBOLS

A	void fraction in the adsorbent bed	–
B	solid fraction in the storage tank	–
B_a	weighting factor for adsorption phenomenon	–
c	heat capacity	$\mathrm{J\,kg^{-1}\,K^{-1}}$
d_p	particle diameter	m
h	convection heat transfer coefficient	$\mathrm{W\,m^{-2}\,K^{-1}}$
K	bed permeability	$\mathrm{m^{-2}}$
k_m	LDF coefficient	$\mathrm{s^{-1}}$
L	length	m
M	molar mass	$\mathrm{kg\,mol^{-1}}$
m	mass	kg
P_d	power density	$\mathrm{W\,m^{-3}}$
p	pressure	Pa
Q_d	energy density	$\mathrm{J\,m^{-3}}$ or $\mathrm{kWh\,m^{-3}}$
$\dot{Q}_v$	airflow rate	$\mathrm{m^3\,s^{-1}}$
q	adsorbed water	$\mathrm{kg_w\,m^{-3}}$
R	gas constant	$\mathrm{J\,K^{-1}\,mol^{-1}}$
S	area	$\mathrm{m^2}$
T	temperature	K
t	time	s
U_b	global heat transfer coefficient	$\mathrm{W\,m^{-2}\,K^{-1}}$
V	volume	$\mathrm{m^3}$
$\vec{u}$	local velocity	$\mathrm{m\,s^{-1}}$
x, y, z, r	coordinate	m

Greek letters

ΔH	Differential heat of sorption	$\mathrm{J\,kg^{-1}}$
ϵ_b	porosity between bead interstices	$-$
ϵ_p	bead internal porosity	$-$
$\vec{\varphi}$	conductive heat flux density	$\mathrm{W\,m^{-2}}$
φ	relative humidity	$-$
γ	multiplication coefficient	$-$
λ	thermal conductivity	$\mathrm{W\,m^{-1}\,K^{-1}}$
μ	dynamic viscosity	$\mathrm{Pa\,s^{-1}}$
ρ	density	$\mathrm{kg\,m^{-3}}$

Subscript

0	initial
b	bed
$conv$	convective
da	dry air
e	equilibrium
end	final
$exch$	exchange
eq	equivalent property
f	fluid
max	maximum
s	solid sorbent
v	water vapor
w	adsorbed water

29

1. Introduction

Currently, physisorption heat storage represents a possible solution for high-energy-density heat storage, especially for building applications [1] (the definition of physisorption can be found in [2]). However, the technological readiness level of this solution remains low and requires advanced research. [3]. The target, identified in [4], is a storage system 4 times more compact than water at the system level for being competitive. [5] also emphasized the necessity to reduce the size of systems and physisorption remains definitely an appropriate solution.

During the last 10 years, researchers have been interested in developing concepts allowing the use of physisorption materials. In most laboratory system developments, the sorbate has been water vapor, and the sorbent has been zeolite:

- ⋆ zeolite 13 X open reactor developed by ZAE Bayern [6],
- ⋆ silica gel closed reactor developed in the framework of the project *Modestore* [7],
- ⋆ zeolite 4A open rotating reactor developedin the framework of the project *Flow-TCS* [8],
- ⋆ zeolite 5A closed reactor developed in the framework of the project *E-hub* [9],
- ⋆ zeolite 13 X open reactor developed by INSA Lyon [10],
- ⋆ zeolite 13 X open reactor developed by TU Eindhoven [11].

In most of the cases, dry air is used as a carrier fluid for water vapor; the mixing of dry air and water vapor is called moist air. On the whole, the technology readiness level of the systems from the literature doesn't exceed 6 [1], except for the 7000 kg of 13X zeolite storage system installed in Munich, Germany [6]. However, extrapolation of experimental results are difficult because of the limitations of test possibility or flexibility. Even if a lot of materials are potential candidates for physisorption heat storage [12], zeolite remains the most studied material because of availability and price.

In parallel with real systems, researchers have also been interested in the numerical modeling of zeolite energy storage. Indeed, the numerical modeling of sorption heat storage systems remains fundamental for 1) optimization, 2) control and 3) energy efficiency assessment. Basically, all the numerical models are based on the same set of partial differential equations:

- ◇ the mass conservation of dry air or moist air and water,
- ◇ the energy conservation of dry air or moist air and solid sorbent,
- ◇ the momentum conservation of dry air or moist air.

Differences in numerical models depend mainly on the variables of interest and the assumption concerning the sorption and diffusion physical phenomena. Mette et al. [13] developed a numerical model of an open zeolite 13 X / moist air storage reactor validated using their own experimental data. The heat and mass transport inside of the reactor was described with a quasi-homogenous model, meaning no temperature difference between the solid and fluid phase. Experimental data were also used to fit some model parameters. The same type of reactor was studied in Gaieni et al. [14]. The

quasi-homogeneous fluid and solid temperature assumption was assumed, as well as the Langmuir isotherm. The effect of the kinetics coefficient on the efficiency of a large scale reactor was also studied. It was found that slower adsorption reduces both the efficiency and the power of the reactor. Smejkal et al. [15] developed a two-temperatures model of a zeolite 13X heat storage and found that the temperature difference between fluid and solid can reach up to 2 K. Unfortunately, the authors did not analyze the parameters sensitivity of their finite-element model. A zeolite / water vapor closed system was studied in Dusquene et al. [16] considering sorption having an instantaneous kinetic. The model is validated using data from the literature but issues about the sorption kinetics are only raised in the conclusions. A similar approach was used in the work of Schaefer and Thess [17, 18] except for the kinetics expressed by a linear driving force model. The authors discussed an optimum of the thermal performance over the channel or particle size. A computational fluid dynamics (CFD) approach was employed in Reichl et al. [19] to model the heat and mass transfers in an open rotating drum. Despite the accuracy of such model, the computational cost and time of CFD eliminates it for control or sensitivity analysis purposes. It is also worth mentioning that composite zeolite / hygroscopic salt has also been studied in the literature, for instance, packed beds of salt / zeolite composites in the work of Lehmann et al. [20] and zeolite 13X / magnesium sulfate in the study of Xu et al. [21]. However, composite materials are out of the scope of the present study as the physical phenomena differ from pure physisorption.

Validated numerical models can also provide substantial information when conducting a sensitivity analysis. One possible definition of sensitivity anal-

ysis is given in Saltelli et al. [22]: *The study of how uncertainty in the output of a model (numerical or otherwise) can be apportioned to different sources of uncertainty in the model input.*. More information can also be found from sensitivity analyses, including, albeit not an exhaustive list,

- Understanding of the relationship between the inputs and outputs of the model,
- Reducing the model complexity by retaining the most important inputs or parameters (also called model reduction), and
- Optimizing the system.

The scientific literature is surprisingly limited concerning the sensitivity analysis of zeolite heat storage systems, even though it has been a subject of interest for other thermal storage technologies: Bonanos et al. [23] for thermocline thermal storage tank design, Woloszyn et al. [24] for rock mass sensible heat storage, Woloszyn et al. [25] for borehole sensible heat storage, Caliano et al. [26] for biomass-fired combined cooling heating and power system with thermal energy storage systems, Zalba et al. [27] for a phase change material (PCM) thermal mass and Kuznik et al. [28] for PCM building walls. In Kamdem et al. [29], a first and simple attempt is presented and concerns only the linear driving force (LDF) parameter, the wall heat transfer coefficient, the mass dispersion coefficient and the effective axial thermal conductivity. The sensitivity analysis is qualitative, and no cross-effects are investigated. The results lead to the conclusion that among the tested parameters, the LDF parameter and the wall heat transfer coefficient have the

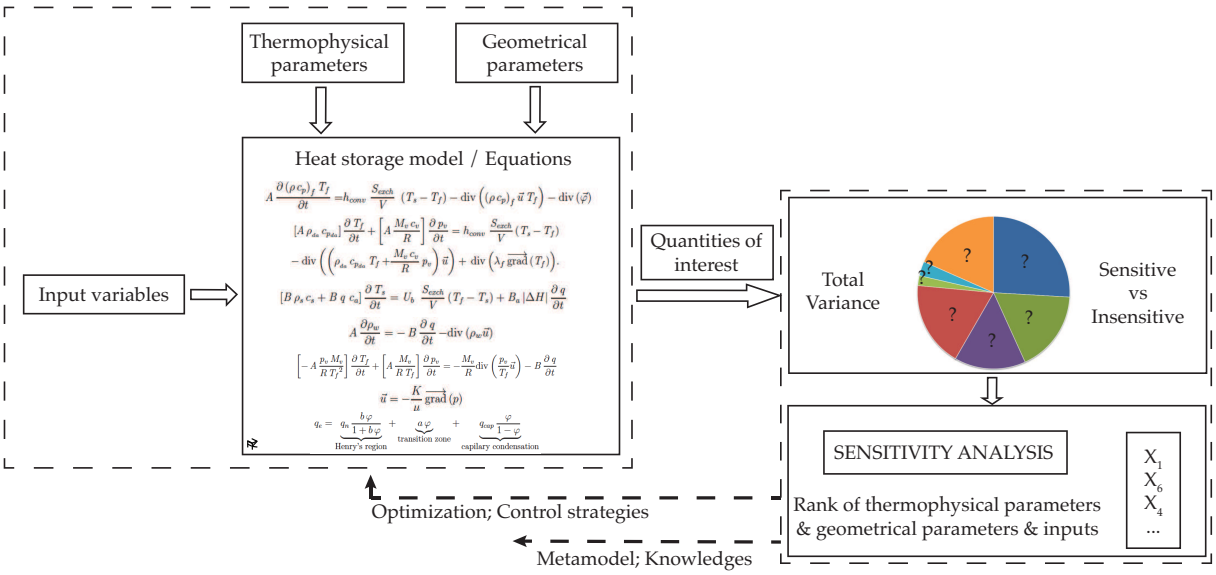

Figure 1: Overall methodology.

strongest influence on the power released. Those results are in agreement with those from Gaieni et al. [14] concerning the reaction kinetics.

We propose to bring additional understanding of open zeolite system by analyzing the parameters and variables related to materials, operating conditions and geometry and their impact on heat storage density and discharge power density. Then, we decided to conduct a systematic sensitivity study based on analysis of variance. The overall methodology developed and carried in the paper is presented in Fig. 1. The system under consideration, i.e., a zeolite heat storage system for the heating of a building, is described in section 2. Note that the experimental analysis of the laboratory prototype of the storage system has been presented in a previous article written by the authors [30]. The numerical model, which is the basis of the analysis, is

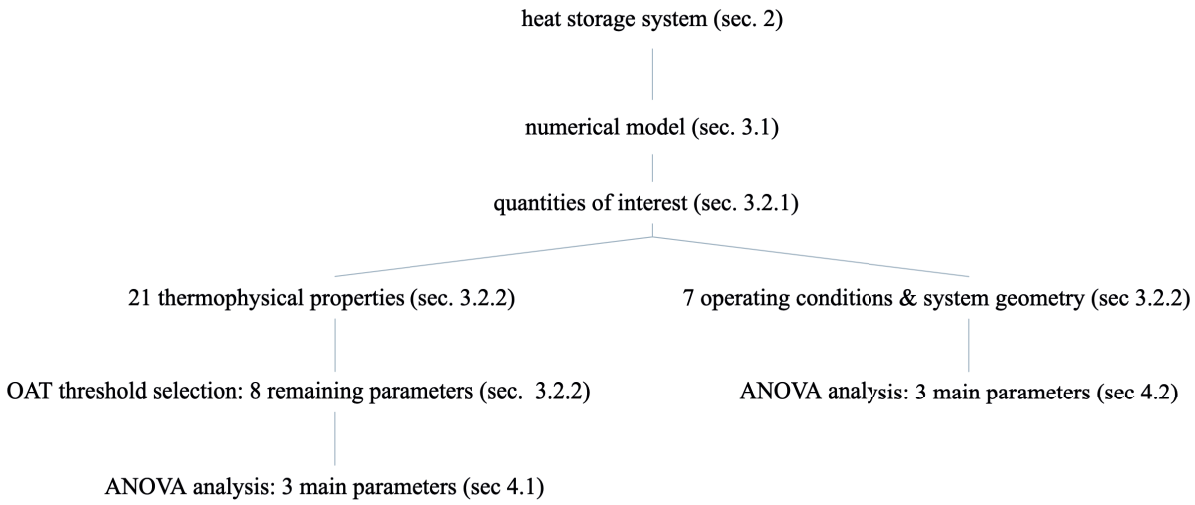

Figure 2: Schematic overview of the article.

presented in section 3.1. More information on the model development, validation and verification can be found in [31]. Only the governing equations are presented in this article. The methodology used for the analysis of variance is presented in section 3.2. The results are presented and discussed in section 4, and the conclusions are given at the end of the paper. The Fig. 2 gives an overview of the article.

2. Description of the thermal energy storage system

Detailed information about the heat storage system, the experimental procedure and the measurements and analysis can be found in [30, 32]. For the sake of understanding, only the most important information is given hereafter.

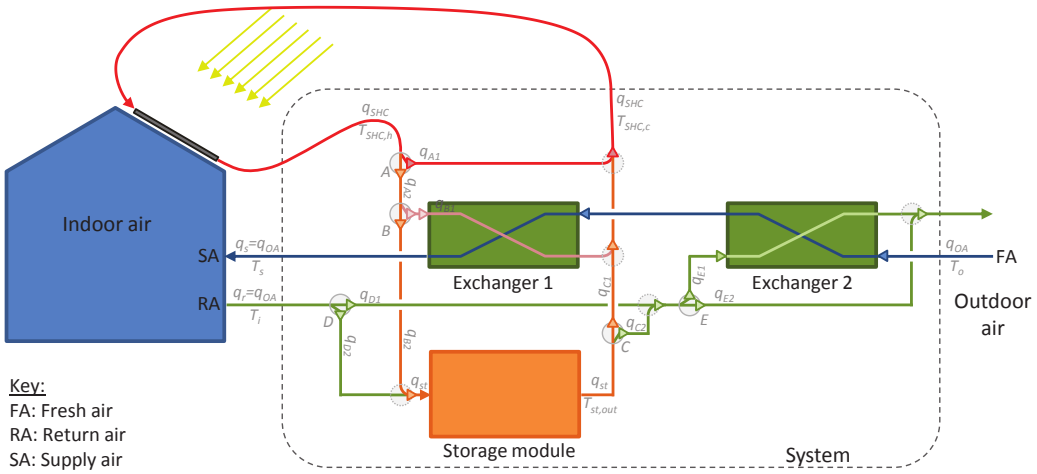

Figure 3: Sketch of the storage system integration in the building.

The purpose of the heat storage system was to shave the peak electricity load occuring in winter at the end of the day, between 6 and 8 PM. For a low-energy house of 100 m^2, the specification requirements become 2 kW [33] during 2 h . The developed strategy consist in integrating the storage in the ventilation system of a single-family house or residential apartment [34, 35]. The integration concept of the storage system is presented in Fig. 3 and the objective is to use, preferably, solar heat. Note that if solar energy is not available, the heat can be supplied by an electrical heater (i.e., resistance) or a heat pump.

The figure Fig. 4 shows the experimental setup. The prototype was initially developed in our laboratory. Basically, it is composed of two reactors in order to test different configurations: serial or parallel. Each reactor is filled with Faujasite zeolite $Na - X$ (Alfa Aesar, $13X$, beads 1.6 mm to 2.5 mm; see Fig. 4a). Basically, one reactor contains 40 kg of zeolite. The geometry of

each reactor is a cylinder 72 cm in diameter, with a bed thickness of 20 cm. At the design stage, the shape of each reactor was optimized to generate a vertical and radially homogeneous air flow (Fig. 4b and4d).

(a) Zeolite beads

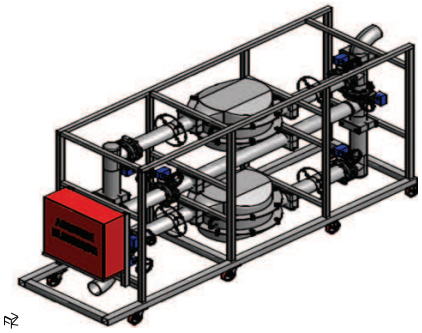

(b) Sketch of the prototype

(c) Experimental setup without insulation

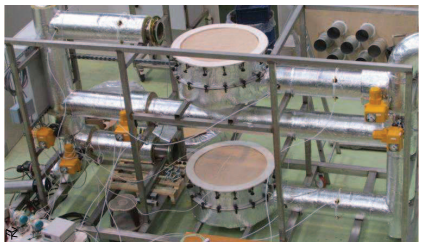

(d) Experimental setup with loaded and opened reactors

Figure 4: Experimental setup.

The insulated reactors were connected to a airflow generator allowing to control the airflow rate at the entrance, as well as the temperature and humidity level (Fig. 4c). The experimental campaign has been designed to address, with a minimum number of tests, the influence of:

- desorption temperature (120 °C vs. 180 °C),
- air flow rate (180 $m^3 h^{-1}$ vs. 90 $m^3 h^{-1}$ vs. 60 $m^3 h^{-1}$),

- relative humidity in discharging mode (50% vs. 70%),
- bed thickness (20 cm vs. 10 cm),
- serial/parallel configurations.

Inlet experimental conditions of all the tests are summarized in Tab. 1: desorption temperature and airflow rate; desorption temperature, aiflow rate and humidity. On the whole, the released heating power is about 27.5 $\mathrm{W\,kg^{-1}}$ [30].

3. Methods

3.1. Governing equations, numerical procedure and validation

The content of this subsection is detailed in [31]. For the sake of understanding, only the most important information is given hereafter.

3.1.1. Governing equations

The domain of the numerical model is the zeolite bed with the metal container. An sketch of the physical domain under consideration is presented in Fig. 5. Because of the cylindrical shape of each reactor, we consider a symmetry around the z axis.

The content of the reactor tank is considered as being 2 medium: the solid and moist/dry air. Solid parts are composed of sorbent material (indicated by the subscript s) and adsorbed water (indicated by the subscript w). The fluid (indicated by the subscript f) is composed of dry air (indicated by the subscript da) and water vapor (indicated by the subscript v).

Two phases, solid and gas, are considered in the reactor, with each phase having their own thermophysical properties, thermodynamical properties and, of course, governing equations. This choice is guided by physical considerations and representativeness of the underlying physics [36].

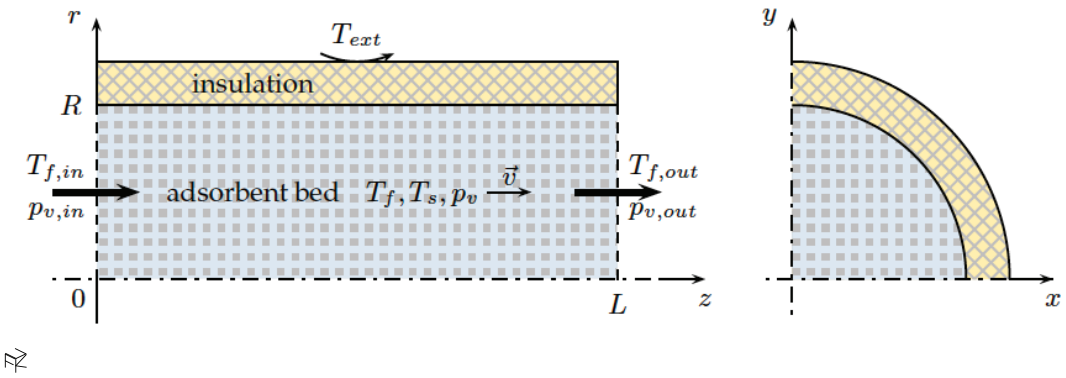

Figure 5: Sketch of the cylindrical reactor.

The energy conservation equation of dry air is given by

$$\begin{aligned}[A\,\rho_{da}\,c_{da}]\,\frac{\partial\,T_f}{\partial t}+\left[A\,\frac{M_v\,c_v}{R}\right]\frac{\partial\,p_v}{\partial t}&=h_{conv}\;\frac{S_{exch}}{V}\,(T_s-T_f)\\ -\,\mathrm{div}\left(\left(\rho_{da}\,c_{da}\,T_f+\frac{M_v\,c_v}{R}\,p_v\right)\vec{u}\right)&+\,\mathrm{div}\left(\lambda_f\,\overrightarrow{\mathrm{grad}}\,(T_f)\right).\end{aligned}\tag{1}$$

The energy conservation equation of the solid can be written in the following form:

$$[B\,\rho_s\,c_s+B\,q\,c_a]\,\frac{\partial\,T_s}{\partial t}=U_b\;\;\frac{S_{exch}}{V}\,(T_f-T_s)+B_a\,|\Delta H|\,\frac{\partial\,q}{\partial t}\tag{2}$$

The water mass conservation equation can be straightforwardly formulated as

$$\left[-\,A\,\frac{p_v\,M_v}{R\,{T_f}^2}\right]\frac{\partial\,T_f}{\partial t}+\left[A\,\frac{M_v}{R\,T_f}\right]\frac{\partial\,p_v}{\partial t}=-\frac{M_v}{R}\mathrm{div}\left(\frac{p_v}{T_f}\vec{u}\right)-B\,\frac{\partial\,q}{\partial t}\tag{3}$$

In the reactor, the worst-case estimation of the Reynolds number is 10.6. Since several overestimations led to this value, assuming that the Reynolds number remains below 10 in the whole adsorbent bed seems reasonable.

Darcy's law is therefore chosen for the calculation of the fluid velocity:

$$\vec{u} = -\frac{K}{\mu} \overrightarrow{\text{grad}}\,(p) \tag{4}$$

where the bed permeability is derived from [37] as:

$$K = \frac{d_p^2\,\epsilon_b^3}{180\,(1-\epsilon_b)^2} \tag{5}$$

d_p being the particles diameter and ϵ_b the bed porosity.

The Linear Driving Force (LDF) model is chosen to approach kinetics. The equation takes the following form:

$$\frac{\partial q}{\partial t} = k_m\,(q_e - q) \tag{6}$$

The adsorption equilibrium model developed in our previous work is expressed as a sum of three terms:

- the Langmuir isotherm for low relative humidity,
- a linear function for the transition region, and
- a term in the BET model for high relative humidity.

$$q_e = \underbrace{q_n \frac{b\,\varphi}{1+b\,\varphi}}_{\text{Henry's region}} + \underbrace{a\,\varphi}_{\text{transition zone}} + \underbrace{q_{cap}\frac{\varphi}{1-\varphi}}_{\text{capillary condensation}} \tag{7}$$

The fitting coefficients for adsorption isotherms are given in [31].

The following correlation is used to obtain the differential enthalpy of adsorption ΔH of zeolite 13X as a function of water uptake Δm_w. It is derived from the polynomial fitting of the zeolite 13X curve given in [38].

$$\begin{aligned}\Delta H = 7.59\times10^{-4}\Delta m_w^5 - 5.34\times10^{-2}\Delta m_w^4 \\ + 1.12\Delta m_w^3 - 2.38\Delta m_w^2 - 186.8\Delta m_w + 4984\end{aligned} \tag{8}$$

3.1.2. Numerical procedure

Space is discretized using the control-volume method in (z, r) coordinates considering z as the symmetry line (see Fig. 5). This strategy is suitable to ensure tye enenrgy balance, the mass balance and the momentum balance locally. The spatial derivatives (gradient, divergence and laplacian) are second-order accurate in space. The velocity et each control-volume boundary is calculated with the staggered grid strategy [39]. An upwind numerical scheme is used to calculate the advection terms. The set of differential equations is solved using Gear's method, i.e. an implicit linear multi-step method based on backward differentiation.

3.1.3. Validation

Given the good agreement between the experimental data and the numerical results, fully presented in [31], the model is considered as fully validated in the following range of operating conditions:

- charging temperature from 120 °C to 180 °C,
- inlet humidity on charge of 30 % at 20 °C,
- inlet humidity on discharge from 50 % at 70 % at 20 °C,
- inlet fluid velocity from $0.01\,\mathrm{m\,s^{-1}}$ at $0.03\,\mathrm{m\,s^{-1}}$, and to a lesser extent for lower inlet fluid velocities.

3.2. Sensitivity analysis

3.2.1. Definition of the quantity of interest (QOI)

When using sensitivity analysis, the first task is to define the outputs or the response variables (the exact term depends on the scientific area). As the

numerical model posses as many outputs as the number of nodes, we prefer defining the observed variable under investigation as the *quantity of interest* (QOI). In the work here, two different QOIs are analyzed:

- the maximum discharge power density, $P_{d,max}$ [W m^{-3}], calculated using the following formula:

$$P_{d,max} = \frac{\dot{Q}_v \times \rho_{da} \times c_{da}}{3600 \times S \times L_z} \times (T_{f_{max}} - T_{f_0}) \tag{9}$$

- the heat storage density, Q_d [kWh m^{-3}], calculated via

$$Q_d = \frac{\dot{Q}_v \times \rho_{da} \times c_{da}}{3600 \times S \times L_z} \times \int_{t_0}^{t_{end}} \left(T_f|_{z=L_z} - T_f|_{z=0} \right) dt \tag{10}$$

Note that other quantities of interest could be defined concerning, for instance, the time characteristics of both charge and discharge phases. However, multiplying the QOI does not change the methodology. The final choice of the QOI strongly depends on the specifications of the heat storage system.

3.2.2. Definition of the parameters

Two families of parameters are investigated: 1) the thermophysical properties and 2) the operating conditions and the system geometry. They are studied independently as this is their underlying nature. When analyzing the thermophysical properties, the objective is two-fold: on the one hand, the identification of parameters requiring careful measurement and, on the other hand, the material optimization possibilities. Concerning the analysis of the operating conditions and geometry, the goal is to understand how these parameters influence the discharge power and the energy density.

Thermophysical properties

Among the thermophysical properties required to model the storage system, the adsorption kinetics and the adsorption equilibrium are curve-shape-dependent parameters (the curves are the equations 7 & 8). Therefore, for the sake of consistency, we have decided to vary these parameters while maintaining the curve shape. Then, 2 parameters are defined: γ_{q_e} and $\gamma_{|\Delta H|}$. Those parameters are multiplication coefficients for the curves representing the sorption kinetics and the sorption equilibrium, respectively. The same technique is also used to assess the LDF parameter k_m and then a multiplication coefficient γ_{k_m} is also introduce in the analysis.

Thermophysical properties are too numerous to consider all possible interactions between variables (more than 25 thermophysical properties!). A filtering step has to be performed first to select the most strongly influential parameters. To achieve a reasonable computation time for the initial screening, we chose to perform a one-at-a-time (OAT) sensitivity analysis. This local technique analyzes the impact of one parameter on the QOI at a time, therein keeping the other parameters fixed. This step enables one to rank parameters from the most influential to the least influential. No interaction effects between factors are considered at this step.

The methodology here consists in a design of experiments set up with three levels: minimum value, default value and maximum value. Based on our expertise, only 21 parameters have been selected. Tab. 2 presents the variation range of the parameters as well as the sensitivity according to the QOI defined previously. The definition of the variation range of the parameters was decided based on expert judgment, i.e., the authors of the present

article. The mean square (abbreviation Mean Sq. in Tab. 2) is an estimate of the population variance. It is calculated by dividing the corresponding sum of squares by the number of degrees of freedom. In the sensitivity analysis, the mean square is used to determine whether factors are significant. Moreover, the mean square value of each factor is compared to the overall mean square value sum into a weighting term (called Weight in Tab. 2).

The results from Tab. 2 show that the seven most influential parameters (overall) are also the seven most influential parameters for both outlet power density and heat storage density. The seventh parameter accounts for 0.9% of the mean square sum for the power density (λ_f) and 1.6% of the mean square sum for the storage density. The eighth parameter ϵ_b still accounts for 0.6% of the mean square sum on the storage density, while all other parameters account for less than 0.1% on both the power and energy densities. It then seems relevant and conservative enough to keep only the top eight most influential parameters from Tab.2 for the analysis of variance carried in section 4.1.

Operating conditions and system geometry

The operating conditions are defined as the controllable parameters. Five parameters are identified as important operating conditions:

- inlet flow rate during charge $\dot{Q}_{in,charge}$ with a variation range of $60\,\mathrm{m^3\,h^{-1}}$ to $250\,\mathrm{m^3\,h^{-1}}$,
- inlet flow rate during discharge $\dot{Q}_{in,discharge}$ with a variation range of $60\,\mathrm{m^3\,h^{-1}}$ to $250\,\mathrm{m^3\,h^{-1}}$,
- charging temperature $T_{in,charge}$ with a variation range of $110\,^{\circ}\mathrm{C}$ to

307 180 °C,

308 • charging humidity ratio $\varphi_{in,charge}$ with a variation range of 0.5% to
309 0.1%,

310 • discharging humidity ratio $\varphi_{in,discharge}$ with a variation range of 50% to
311 80%.

312 The volume and shape of the adsorbent bed necessarily have an influ-
313 ence on the QOI. However, it seems wise to conduct an operating condition
314 study and geometrical study together since they can influence each other.
315 The influences of the bed length L_z and cross-sectional area S are thus also
316 investigated with variation ranges of 40 cm to 10 cm and of 0.2 m^2 to 0.8 m^2,
317 respectively.

318 *3.2.3. Methodology*

319 Analysis of variance (ANOVA) applied to sensitivity analysis allows to as-
320 sess the main effects of each parameter on the overall variance (i.e., the sum
321 of the squared differences between each simulation and the overall mean). In
322 contrast to the OAT sensitivity analysis, ANOVA can also assess the inter-
323 actions between factors. Additional details on the application of ANOVA to
324 sensitivity analysis, including the mathematical and technical background,
325 can be found in [22, 40].

326 Analysis of variance is based on a 2^k full factorial design of experiment.
327 It means that all possible combinations between two levels (low and high) of
328 each of the k parameters are run. A full factorial design enables to examine
329 the influence of main effects (as in OAT analysis) but also the influence of
330 all interaction effects between groups of two variables. This can technically

be achieved on *Matlab*® by using the N-way analysis of variance function *anovan* from the Statistics Toolbox, with the *interactions* model.

4. Results and discussion

4.1. Analysis of variance: thermophysical properties

The results from the analysis of variance are given in Tab. 3. They are ranked by descending order of influence.

The mean squares represent an estimate of the population variances. They are calculated by dividing the corresponding sum of squares by the degrees of freedom (called Mean Sq. in Tab. 3). In analysis of variance, the mean squares are used to determine whether factors are significant or not. The ANOVA-based sensitivity index of a parameter can be defined as the ratio of the sum of its squares to the total sum of squares. This is called Weight in Tab. 3. The overall weight value (called Overall weight in Tab. 3) is calculated by averaging the weight values on the outlet power density and storage density. Only the most influential interactions are presented in the table. The leftover weight is calculated as the sum of the remaining terms (called Left over in Tab. 3).

Note that in Tab. 3, weights can only be compared by column, not by rows. For instance, a higher weight on power density compared to on storage density does not mean the influence of $|\Delta H|$ on power is stronger than the influence on storage density. It only reveals weaker contributions of the other parameters on the power density.

It is clear from Tab. 3 that the most influential parameters are the heat of adsorption, the water vapor molar mass and the adsorption equilibrium: their

added contributions, including interactions, represent more than 90% of the ANOVA sensitivity index for both QOIs. The importance of the interactions between these 3 parameters demonstrates the necessity to adopt a variance-based sensitivity method. To quantify the sensitivity of each parameter, Tab. 4 shows the increase or decrease in the QOI when the parameters are varying from their minimum value to their maximum value: a positive value means an increase in the QOI, whereas a negative value means a decrease.

The strong influence of the differential heat of sorption $|\Delta H|$ on both the storage density and power is greater than expected. Table 4 shows that there is a 39.7% increase in outlet power when $|\Delta H|$ varies from 50% to 150% of its default value. The increase in storage density is even higher, i.e., +47.4%!

The second most influential parameter is the vapor molar mass M_v. This parameter is very well known and precisely measured in the literature and therefore not intended to vary if water is used as a fluid. However, this parameter is used in the calculation of the water vapor density ρ_v. It thus shows that the vapor density strongly influences the results. It also means that changing the sorbate can be an option to increase the energy and power densities.

The adsorption equilibrium is a function of the fluid temperature and pressure; thus, it is not a direct parameter. To assess the influence of high or low equilibrium values on the results, a weighting factor is used to artificially modify q_e: γ_{q_e}. Table 4 shows that q_e has a stronger influence on the storage density (+42.3% when q_e changes from 50% to 150% of its default value) than on the outlet power (+5.6%).

Clearly, c_a has an influence on the heat releasable to the system. Indeed,

a quantity $|\Delta H|$ is released on adsorption. However, this reaction requires a water molecule to be turned from vapor to the adsorbed state. The energy contained in the vapor phase is proportional to the product of the vapor heat capacity c_v and fluid temperature T_f. But, the energy contained in the adsorbed layer is proportional to the adsorbed layer heat capacity c_a and the solid temperature T_s. An amount $c_a \times T_s - c_v \times T_f$ is then provided to the water vapor to transform it to the adsorbed phase. In other words, the net amount of heat released in adsorption is $|\Delta H| - (c_a\ T_s - c_v\ T_f)$. Consequently, the higher c_a is, the more energy required to trigger the adsorption reaction, the lower the net heat released.

Experiments are performed with a low value of $c_v = 1000\,\mathrm{J\,kg^{-1}\,K^{-1}}$ and a high value of $c_v = 4000\,\mathrm{J\,kg^{-1}\,K^{-1}}$. The same comment on the water molar mass is necessary: the goal here is not to address the influence of small changes in water vapor mass but rather to evaluate, for instance, the importance of considering its variation with temperature changes. The goal is also to address the influence of the fluid heat capacity to investigate the opportunity to use another fluid. The results from Tab. 4 show that the vapor heat capacity influences the energy storage density (+9.8%) and outlet power (8.6%). The same considerations as for the interpretation of the adsorbed layer heat capacity influence are relevant. With a higher c_v and the same inlet temperature, the energy gap from the vapor to adsorbed phase is lower. The net heat released on adsorption is consequently higher.

In this study, the fluid thermal conductivity was strongly varied from a very low value ($0.025\,\mathrm{W\,m^{-1}\,K^{-1}}$) to a very high value ($1.0\,\mathrm{W\,m^{-1}\,K^{-1}}$). Surprisingly, this very large variation range does not lead to significant changes

in outlet power or storage densities. Diffusion does not require mass transport and is proportional to λ_f, and advection relies on mass transport (and hence fluid velocity). In charging and discharging modes, the advection term is approximately 500-times greater than the diffusion term. Thus, it is not surprising that it does not influence the results much (-4.0% on power and $+0.8\%$ on storage density, with a high value 40-times larger than the low value).

Investigations on the solid density influence have been conducted with a low value of $600\,\mathrm{kg\,m^{-3}}$ and a high value of $1500\,\mathrm{kg\,m^{-3}}$. Table 4 shows that ρ_s has a quiet weak influence on the outlet power (-3.1% from low to high values) but has a stronger influence on the storage density (-10.4%). A high solid density tends to limit the temperature drop within the solid and hence the temperature drop within the fluid. This explains why the outlet power is limited by the high solid density.

The bed porosity influence is investigated with a low value $\epsilon_b = 0.32$ and high value $\epsilon_b = 0.40$. Table 4 shows that the influence of ϵ_b on the outlet power is quiet negligible (-0.9%), whereas it is more important on the storage density (-5.7%). ϵ_b has a direct influence on the fluid/solid volume ratio, as well as on the exchange surface between fluid and solid. A higher ϵ_b tends to lower the exchange surface, increase the fluid volume and decrease the solid volume.

4.2. Analysis of variance: operating conditions and system geometry

The results from the analysis of variance are given in Tab. 5. The analysis indices are similar to those defined in the previous section. The parameters are ranked in descending order of influence. The main influential parameters

are the inlet relative humidity, the bed length and the inlet fluid flow rate: their contributions, including interactions, represent more than 92% of the ANOVA sensitivity index for both energy density and power density. Table 6 shows the increase or decrease in the QOIs when the parameters are varying from their minimum value to their maximum value.

The inlet relative humidity has a strong influence on the results in both charge and discharge phases. In the present case, Tab. 6 shows a $13.2\,\mathrm{kWh\,m^{-3}}$ (17.9%) and $12.4\,\mathrm{kWh\,m^{-3}}$ (16.8%) storage density difference for the charge and discharge inlet relative humidity, respectively. The outlet power density is also changed in approximately the same proportions (12.5% on charge and 24.2% on discharge).

The inlet flow rate is an operating condition that has a strong influence on system behavior and can be easily adjusted. Table 6 shows that the inlet flow rate has few influence on the energy storage density (i.e., +2.2%). However, the outlet power is strongly influenced by the inlet flow rate: +61.4% from $60\,\mathrm{m^3\,h^{-1}}$ to $250\,\mathrm{m^3\,h^{-1}}$ equivalent. An increase in the inlet flow rate during discharge increases the water vapor in the system. As the reaction kinetics are fast enough and the bed long enough to adsorb all incoming water molecules, the adsorption sites are filled faster.

Adsorption equilibrium depends on temperature and vapor pressure. At high temperature, molecular agitation is higher, and the adsorbed layer density is lower. The inlet temperature during charging has a strong influence on the adsorption equilibrium and hence the system charge. A higher charging temperature is expected to allow a dryer final charging state. The heat storage density increases by +5.1% within the studied temperature range.

The outlet power density is decreasing, i.e., -12.5%, because of obvious interactions between $\varphi_{in,charge}$ and $T_{f,in,charge}$.

The bed geometry, defined by the bed length L_z and cross-sectional area S, is investigated jointly for the sake of being thorough. The results clearly show a strong correlation between bed length and outlet power density. A shorter bed provides a higher power density ($+61.3\%$ from 40 cm to 10 cm). The influence on the heat storage density is only 2.8%. For a narrow bed ($S = 0.2\,\mathrm{m}^2$) and for a large bed ($S = 0.8\,\mathrm{m}^2$), the results of Tabs. 5 and 6 show that the cross-sectional area has no influence in all results.

5. Conclusions

The work presented in the article is one of the first attempt to carry a systematic, extensive, sensitivity analysis of a zeolite heat storage model. The influence of twenty one parameters, five operating conditions and two geometric characteristics on heat storage density and discharge power density has been addressed. The following guidelines must be followed for material development, system design and control strategy optimization.

⇒ The most influential thermophysical properties are the heat of adsorption, the water vapor molar mass and the adsorption equilibrium: their added contributions, including interactions, represent more than 90 % of the sensitivity index for both QOIs.

- The differential heat of sorption $|\Delta \mathrm{H}|$ is the most influencing parameter for the two quantities of interest. The linear increase is 0.4 % and 0.48 % per percentage of $|\Delta \mathrm{H}|$ increase for, respectively, the power density and the energy density.

- The fluid density, the second most influencing parameter, is also to be maximized to benefit the power and energy storage densities.
- The adsorption capacity q_e is a key parameter that is also to be maximized. Nevertheless, the highest outlet power densities are obtained at low q_e values, to the detriment of the storage density. The linear increase is 0.42 % and 0.06 % per percentage of q_e increase for, respectively, the energy density and the power density.

$\Rightarrow$ The most influential operating conditions and system geometry parameter are the inlet relative humidity, the bed length and the inlet fluid flow rate: their added contributions, including interactions, represent more than 92 % of the sensitivity index for both QOIs.

- The most influential parameter is the inlet relative humidity. During the charge phase, the decrease is 12.5 % and 17.9 % for a variation range of $\varphi_{in,charge}$ between 0.1 % to 0.5 % and for, respectively, the power density and the energy density. During the discharge phase, the increase is 24.0 % to 16.8 % for a variation range of $\varphi_{in,discharge}$ between 50 % and 80 % and for, respectively, the power density and the energy density. Then, the difference between the inlet relative humidity on charge and discharge is to be maximized to maximize the QOIs.
- The inlet flow rate strongly influences the time characteristics. A higher inlet flow rate on charge mostly reduces the charging time but few the QOIs. The inlet flow rate on discharge strongly increases the outlet power at the cost of system autonomy. During

the charge phase, the increase in QOIs doesn't exceed 2.2 % for a variation range of $\dot{Q}_{in,charge}$ between $60\,\mathrm{m^3\,h^{-1}}$ to $250\,\mathrm{m^3\,h^{-1}}$ and for the power density and the energy density. During the discharge phase, the increase is 61.4 % and 2.2 % for a variation range of $\dot{Q}_{in,discharge}$ between $60\,\mathrm{m^3\,h^{-1}}$ to $250\,\mathrm{m^3\,h^{-1}}$ and for, respectively, the power density and the energy density.

- The bed length has a strong influence on the power density, a shorter bed being preferable.

There are two main limitations underlying this study. The first one is the model by itself: the choices concerning the physical phenomena representation limit the work to the model presented in the article and, consequently, to the configuration under consideration. No doubt that a closed heat storage system would lead to different conclusions. The second limitation is related to the range of variation of the parameters given in section 3.2.2.

From the results given in section 4, it is possible to determine the most influential parameters depending on the QOI: this is an interesting starting point for the development of a metamodel of the system. Based on the results of section 4, it is possible to keep 3 thermophysical properties and 3 operating conditions and system geometry parameters to derive the metamodel. Such metamodel is usually designed to be fast and accurate and can be an interesting solution for thermal energy storage real-time control.

Acknowledgments

The work presented in this paper has partially received funding from the European Union's Seventh Framework Programme ($FP7/2007-2013$)

under grant agreement $n°PIRSES-GA-2013-610692$ (INNOSTORAGE). This project has also received funding from the *European Union's Horizon 2020 research and innovation programme* under grant agreement no. 657466 (INPATH-TES). This project was also funded by the STAID 2010 project of the ANR-StockE program of the French National Research Agency and supported by the French competitive clusters AXELERA and TENERRDIS.

References

[1] F. Kuznik, K. Johannes, C. Obrecht, D. David, A review on recent developments in physisorption thermal energy storage for building applications, Renewable and Sustainable Energy Reviews 94 (2018) 576–586.

[2] A. D. Mcnaught, A. Wilkinson, IUPAC. Compendium of Chemical Terminology, 2nd ed. (the "Gold Book"), Wiley Blackwell; 2nd Revised edition.

[3] Advanced storage concepts for solar and low energy buildings, Tech. rep., IEA Solar Heating and Cooling Programme – Task 32 (2007).

[4] RHC, Solar heating and cooling – technology roadmap, Tech. rep., Renewable Heating and Cooling – European Technology Platform (2014).

[5] EASE, Thermal storage position paper, Tech. rep., European Association for Stoarge of Energy (2017).

[6] A. Hauer, Adsoprtion systems for TES – design and demonstration projects, in: H. Ö. Paksoy (Ed.), Thermal Energy Storage for Sustain-

able Energy Consumption, Vol. 234, Springer Netherlands, Dordrecht, 2007, pp. 409–427.

[7] C. Bales, P. Gantenbein, D. Jaenig, H. Kerskes, K. Summer, M. van Essen, others, Laboratory tests of chemical reactions and prototype sorption storage units, A Report of IEA Solar Heating and Cooling programme-Task 32.

[8] B. Zettl, G. Englmair, G. Steinmaurer, Development of a revolving drum reactor for open-sorption heat storage processes, Applied Thermal Engineering 70 (1) (2014) 42 – 49.

[9] C. Finck, E. Henquet, C. van Soest, H. Oversloot, A.-J. de Jong, R. Cuypers, H. Spijker, Experimental results of a 3 kW h thermochemical heat storage module for space heating application, Energy Procedia 48 (2014) 320 – 326.

[10] K. Johannes, F. Kuznik, J.-L. Hubert, F. Durier, C. Obrecht, Design and characterisation of a high powered energy dense zeolite thermal energy storage system for buildings, Applied Energy 159 (2015) 80 – 86.

[11] R. van Alebeek, L. Scapino, M. Beving, M. Gaeini, C. Rindt, H. Zondag, Investigation of a household-scale open sorption energy storage system based on the zeolite 13x/water reacting pair, Applied Thermal Engineering 139 (2018) 325 – 333.

[12] S. K. Henninger, S.-J. Ernst, L. Gordeeva, P. Bendix, D. Frohlich, A. D. Grekova, L. Bonaccorsi, Y. Aristov, J. Jaenchen, New materials for adsorption heat transformation and storage, Renewable Energy 110 (2017)

59–68, increasing the renewable share for heating and cooling by the means of sorption heat pumps and chillers.

[13] B. Mette, H. Kerskes, H. Drück, H. Müller-Steinhagen, Experimental and numerical investigations on the water vapor adsorption isotherms and kinetics of binderless zeolite 13x, International Journal of Heat and Mass Transfer 71 (2014) 555 – 561.

[14] M. Gaeini, H. Zondag, C. Rindt, Effect of kinetics on the thermal performance of a sorption heat storage reactor, Applied Thermal Engineering 102 (2016) 520 – 531.

[15] T. Smejkal, J. Mikyska, R. Fucik, Numerical modelling of adsorption and desorption of water vapor in zeolite 13x using a two–temperature model and mixed–hybrid finite element method numerical solver, International Journal of Heat and Mass Transfer (2019) 119050.

[16] M. Duquesne, J. Toutain, A. Sempey, S. Ginestet, E. P. del Barrio, Modeling of a nonlinear thermochemical energy storage by adsorption on zeolites, Applied Thermal Engineering 71 (1) (2014) 469 – 480.

[17] M. Schaefer, A. Thess, Modeling and simulation of closed low-pressure zeolite adsorbers for thermal energy storage, International Journal of Heat and Mass Transfer 139 (2019) 685–699.

[18] M. Schaefer, A. Thess, One-dimensional model of a closed low-pressure adsorber for thermal energy storage, International Journal of Heat and Mass Transfer 117 (2018) 571–583.

[19] C. Reichl, D. Lager, G. Englmair, B. Zettl, M. Popovac, Fluid dynamics simulations for an open-sorption heat storage drum reactor based on thermophysical kinetics and experimental observations, Applied Thermal Engineering 107 (2016) 994 – 1007.

[20] C. Lehmann, O. Kolditz, T. Nagel, Modelling sorption equilibria and kinetics in numerical simulations of dynamic sorption experiments in packed beds of salt/zeolite composites for thermochemical energy storage, International Journal of Heat and Mass Transfer 128 (2019) 1102–1113.

[21] S. Xu, Lemington, R. Wang, L. Wang, J. Zhu, A zeolite 13x / magnesium sulfate–water sorption thermal energy storage device for domestic heating, Energy Conversion and Management 171 (2018) 98–109.

[22] A. Saltelli, M. R. andTerry Andres, F. Campolongo, J. Cariboni, D. Gatelli, M. Saisana, S. Tarantola, Global sensitivity analysis: the primer, John Wiley, 2008.

[23] A. Bonanos, E. Votyakov, Sensitivity analysis for thermocline thermal storage tank design, Renewable Energy 99 (2016) 764 –771.

[24] J. Woloszyn, A. Golas, Sensitivity analysis of efficiency thermal energy storage on selected rock mass and grout parameters using design of experiment method, Energy Conversion and Management 87 (2014) 1297–1304.

[25] J. Woloszyn, Global sensitivity analysis of borehole thermal energy stor-

age efficiency on the heat exchanger arrangement, Energy Conversion and Management 166 (2018) 106–119.

[26] M. Caliano, N. Bianco, G. Graditi, L. Mongibello, Design optimization and sensitivity analysis of a biomass-fired combined cooling, heating and power system with thermal energy storage systems, Energy Conversion and Management 149 (2017) 631–645.

[27] B. Zalba, B. Sanchez, J. M. Marin, An experimental study of thermal energy storage with phase change materials by design of experiments, Journal of Applied Statistics 32 (4) (2005) 321–332.

[28] F. Kuznik, J. P. A. Lopez, D. Baillis, K. Johannes, Phase change material wall optimization for heating using metamodeling, Energy and Buildings 106 (2015) 216 –224.

[29] S. M. Kamdem, K. Johannes, F. Kuznik, H. Bouia, J. J. Roux, Sensitivity analysis of the energy density in a thermo chemical heat storage device, Energy Procedia 48 (2014) 405 –412, proceedings of the 2nd International Conference on Solar Heating and Cooling for Buildings and Industry (SHC 2013).

[30] K. Johannes, F. Kuznik, J.-L. Hubert, F. Durier, C. Obrecht, Design and characterisation of a high powered energy dense zeolite thermal energy storage system for buildings, Applied Energy 159.

[31] F. Kuznik, D. Gondre, K. Johannes, C. Obrecht, D. David, Numerical modelling and investigations on a full–scale zeolite 13x open heat storage for buildings, Renewable Energy 132 (2019) 761–772.

[32] P. Tatsidjodoung, N. Le Pierrès, J. Heintz, D. Lagre, L. Luo, F. Durier, Experimental and numerical investigations of a zeolite 13X/water reactor for solar heat storage in buildings, Energy Conversion and Management 108 (2016) 488–500.

[33] K. Belz, F. Kuznik, K. F. Werner, T. Schmidt, W. K. L. Ruck, 17 - Thermal energy storage systems for heating and hot water in residential buildings, 2015.

[34] V. Bricka, F. Kuznik, K. Johannes, J. Virgone, Evaluation of thermal energy storage potential in low-energy buildings in France, in: 30th ISES Biennial Solar World Congress 2011, SWC 2011, Vol. 3, 2011, pp. 1796–1805.

[35] D. Gondre, K. Johannes, F. Kuznik, Specification requirements for inter-seasonal heat storage systems in a low energy residential house, Energy Conversion and Management 77.

[36] A. Mhimid, Theoretical study of heat and mass transfer in a zeolite bed during water desorption: validity of local thermal equilibrium assumption, International Journal of Heat and Mass Transfer 41 (19) (1998) 2967–2977.

[37] P. C. Carman, Flow of gases through porous media, Academic press, 1956.

[38] C. Bales, P. Gantenbein, A. Hauer, H.-M. Henning, D. Jaenig, H. Kerskes, T. Núñez, K. Visscher, Thermal Properties of Materials for

660 Thermo-chemical Storage of Solar Heat, A Report of IEA Solar Heating
661 and Cooling programme–Task 32.

662 [39] S. V. Patankar, Numerical heat transfer and fluid flow, Hemisphere Pub.
663 Corp. ; McGraw-Hill, Washington; New York, 1980.

664 [40] V. Ginot, S. Gaba, R. Beaudouin, F. Aries, H. Monod, Combined use
665 of local and anovabased global sensitivity analyses for the investigation
666 of a stochastic dynamic model: Application to the case study of an
667 individual-based model of a fish population, Ecological Modelling 193 (3)
668 (2006) 479 –491.

Table 1: Experimental configurations.

Configuration			**Desorption (charge)**			**Adsorption (discharge)**			
S: Series		$m_{adsorbent}$	**Ref.**	$T_{f_{in}}$	$\dot{Q}_{v_{in}}$	**Ref.**	$T_{f_{in}}$	φ_{in}	$\dot{Q}_{v_{in}}$
P: Parallel		kg_z		°C	$m^3\,h^{-1}$		°C	%	$m^3\,h^{-1}$
1	1	40	**1H**	180	180	**1D**	20	70	180
2	2P	40	**2H**	180	90	**2D**	20	70	90
3	2P/2S	40	**3H**	180	180	**3D**	20	70	180
4	2P	40	**4H**	120	90	**4D**	20	70	90
5	2P	40	**5H**	120	90	**5D**	20	50	90
6	2S	40	**6H**	120	180	**6D**	20	70	180
7	1	20	**7H**	180	180	**7D**	20	70	180
8	2P	40	**8H**	180	60	**8D**	20	70	60

Table 2: List of thermophysical properties inventoried with default, minimum and maximum values, and influence weight on maximum outlet power density and energy storage density

Rank	Parameter	Units	Values			Power density		Storage density	
			Default	Min	Max	Mean Sq.	Weight	Mean Sq.	Weight
1	$\gamma_{\lvert\Delta H\rvert}$	% $^{\text{default}}_{\text{value}}$	100%	50%	150%	41.19	53.3%	2680.6	34.8%
2	M_v	$\mathrm{kg\,mol^{-1}}$	0.018	0.012	0.040	23.3	30.2%	3020.6	39.2%
3	γ_{q_e}	% $^{\text{default}}_{\text{value}}$	100%	50%	150%	3.52	4.6%	1344.2	17.4%
4	c_a	$\mathrm{J\,kg^{-1}\,K^{-1}}$	2000	1000	4180	3.22	4.2%	218.3	2.8%
5	c_v	$\mathrm{J\,kg^{-1}\,K^{-1}}$	2000	1000	4000	2.49	3.2%	179.5	2.3%
6	ρ_s	$\mathrm{kg\,m^{-3}}$	760	600	1500	2.69	3.5%	99.2	1.3%
7	λ_f	$\mathrm{W\,m^{-1}\,K^{-1}}$	0.025	0.025	1.00	0.72	0.9%	122.2	1.6%
8	ϵ_b	–	0.37	0.32	0.40	0.0003	0.0%	42.55	0.6%
9	c_s	$\mathrm{J\,kg^{-1}\,K^{-1}}$	1200	500	1500	0.040	0.1%	0.00	0.0%
10	λ_b	$\mathrm{W\,m^{-2}\,K^{-1}}$	0.10	0.02	0.50	0.024	0.0%	0.49	0.0%
11	γ_{k_m}	% $^{\text{default}}_{\text{value}}$	100%	50%	150%	0.020	0.0%	0.04	0.0%
12	c_{da}	$\mathrm{J\,kg^{-1}\,K^{-1}}$	1000	700	1300	0.0022	0.0%	0.54	0.0%

Note: Other investigated parameters are the bead diameter d_p, particle porosity ϵ_p, dry air density ρ_{da}, heat transfer coefficient U_b (whose value is probably too high to lie in a range with tangible effects), moist air dynamic viscosity μ_f and insulation properties such as the insulation thickness e_i, conductivity λ_i and convective heat transfer coefficient on the inner and outer wall $h_{conv,int}$ and $h_{conv,ext}$. The mean square values for all 9 coefficients are very low for both outlet power density (≤ 0.0007) and storage density (≤ 0.11).

Table 3: Analysis of variance on outlet power density and heat storage density for selected thermophysical properties

Rank	Num.	Factor	Power density		Energy density		Overall	Left
			Mean Sq.	Weight	Mean Sq.	Weight	weight	over
1	1	$\gamma_{\Delta H}$	2742.8	54.8%	131392.9	28.0%	41.4%	58.6%
2	2	M_v	741.9	14.8%	127006.1	27.1%	20.9%	37.7%
3	3	γ_{q_e}	65.7	1.3%	104919.2	22.4%	11.8%	25.8%
4	1x2	$\gamma_{\lvert\Delta H\rvert} \times M_v$	567.7	11.3%	29627.8	6.3%	8.8%	17.0%
5	2x3	$M_v \times \gamma_{q_e}$	252.3	5.0%	21780.0	4.6%	4.8%	12.2%
6	1x3	$\gamma_{\lvert\Delta H\rvert} \times \gamma_{q_e}$	0.2	0.0%	20768.1	4.4%	2.2%	9.9%
7	4	c_a	148.5	3.0%	6713.7	1.4%	2.2%	7.7%
8	5	c_v	145.7	2.9%	5616.9	1.2%	2.1%	5.7%
9	2x6	$M_v \times \rho_s$	138.3	2.8%	166.8	0.0%	1.4%	4.3%
10	3x7	$\gamma_{q_e} \times \rho_s$	87.2	1.7%	604.6	0.1%	0.9%	3.4%
11	6	λ_f	10.1	0.2%	6291.1	1.3%	0.8%	2.6%
12	2x5	$M_v \times c_v$	39.8	0.8%	2231.6	0.5%	0.6%	1.9%
13	2x4	$M_v \times c_a$	31.6	0.6%	1822.8	0.4%	0.5%	1.4%
14	2x6	$M_v \times \lambda_f$	3.0	0.1%	2281.9	0.5%	0.3%	1.2%
15	7	ρ_s	19.0	0.4%	36.4	0.0%	0.2%	1.0%
16	1x6	$\gamma_{\lvert\Delta H\rvert} \times \lambda_f$	0.4	0.0%	1528.5	0.3%	0.2%	0.8%
17	8	ϵ_b	0.7	0.0%	1408.2	0.3%	0.2%	0.6%

Table 4: Mean difference on outlet power density and heat storage density between sets of maximum physical parameter values and sets of minimum physical parameter values

Factor		**Power density**		**Storage Density**	
		$\mathrm{kW\,m^{-3}}$	%	$\mathrm{kWh\,m^{-3}}$	%
1	$\gamma_{\lvert\Delta H\rvert}$	3.2	39.7%	22.6	47.4%
2	M_v	1.7	21.2%	22.6	47.3%
3	γ_{q_e}	0.5	5.6%	20.2	42.3%
4	c_a	−0.8	−10.0%	−5.8	−12.0%
5	c_v	0.7	8.6%	4.7	9.8%
6	λ_f	−0.3	−4.0%	0.4	0.8%
7	ρ_s	−0.3	−3.1%	−5.0	−10.4%
8	ϵ_b	−0.1	−0.9%	−2.7	−5.7%

Table 5: Analysis of variance on outlet power density and heat storage density under different operating conditions

		Factor	Power density		Energy density		Overall	Left
			Mean Sq.	Weight	Mean Sq.	Weight	weight	over
1	1	$\varphi_{in,charge}$	1187.9	1.5%	22256.1	43.9%	22.7%	77.3%
2	2	$\varphi_{in,discharge}$	4467.8	5.5%	19706.2	38.8%	22.2%	55.1%
3	3	L_z	28697.4	35.6%	534.1	1.1%	18.3%	36.8%
4	4	$v_{in,discharge}$	28782	35.7%	342.9	0.7%	18.2%	18.6%
5	3x4	$L_z \times v_{in,charge}$	10752.4	13.4%	51.4	0.1%	6.7%	11.9%
6	1x5	$\varphi_{in,charge} \times T_{f,in,charge}$	91.7	0.1%	4342.1	8.6%	4.3%	7.5%
7	5	$T_{f,in,charge}$	1198.8	1.5%	1847.7	3.6%	2.6%	5%
8	2x4	$\varphi_{in,discharge} \times v_{in,charge}$	1670.8	2.1%	274.8	0.5%	1.3%	3.7%
9	2x3	$\varphi_{in,discharge} \times L_z$	1667.5	2.1%	40.2	0.1%	1.1%	2.6%
10	3x5	$L_z \times T_{f,in,charge}$	529.6	0.7%	82.3	0.2%	0.4%	2.2%
11	1x3	$\varphi_{in,charge} \times L_z$	496.7	0.6%	87	0.2%	0.4%	1.8%
12	6	$v_{in,charge}$	3.5	0.0%	337.4	0.7%	0.3%	1.5%
13	3x6	$L_z \times v_{in,discharge}$	3.3	0.0%	331.4	0.7%	0.3%	1.1%
14	4x5	$v_{in,charge} \times T_{f,in,charge}$	442.1	0.5%	34.3	0.1%	0.3%	0.8%
15	2x5	$\varphi_{in,discharge} \times T_{f,in,charge}$	48.3	0.1%	268.4	0.5%	0.3%	0.5%
16	1x6	$\varphi_{in,charge} \times v_{in,charge}$	446.1	0.6%	0.3	0.0%	0.3%	0.2%
21	7	S	0.1	0.0%	0.5	0.0%	0.0%	0.0%

Table 6: Mean difference on outlet power density and heat storage density between sets of maximum operating condition parameter values and sets of minimum operating condition parameter values

	Factor	**Power density**		**Storage density**	
		$\mathrm{kW\,m^{-3}}$	%	$\mathrm{kWh\,m^{-3}}$	%
1	$\varphi_{in,charge}$	−3.0	−12.5%	−13.2	−17.9%
2	$\varphi_{in,discharge}$	5.9	+24.2%	12.4	+16.8%
3	L_z	−15.0	−61.3%	−2.0	−2.8%
4	$v_{in,discharge}$	15.0	+61.4%	1.6	+2.2%
5	$T_{in,charge}$	−3.1	−12.5%	3.8	+5.1%
6	$v_{in,charge}$	0.17	+0.7%	1.6	+2.2%
7	S	0.02	+0.1%	0.07	+0.1%

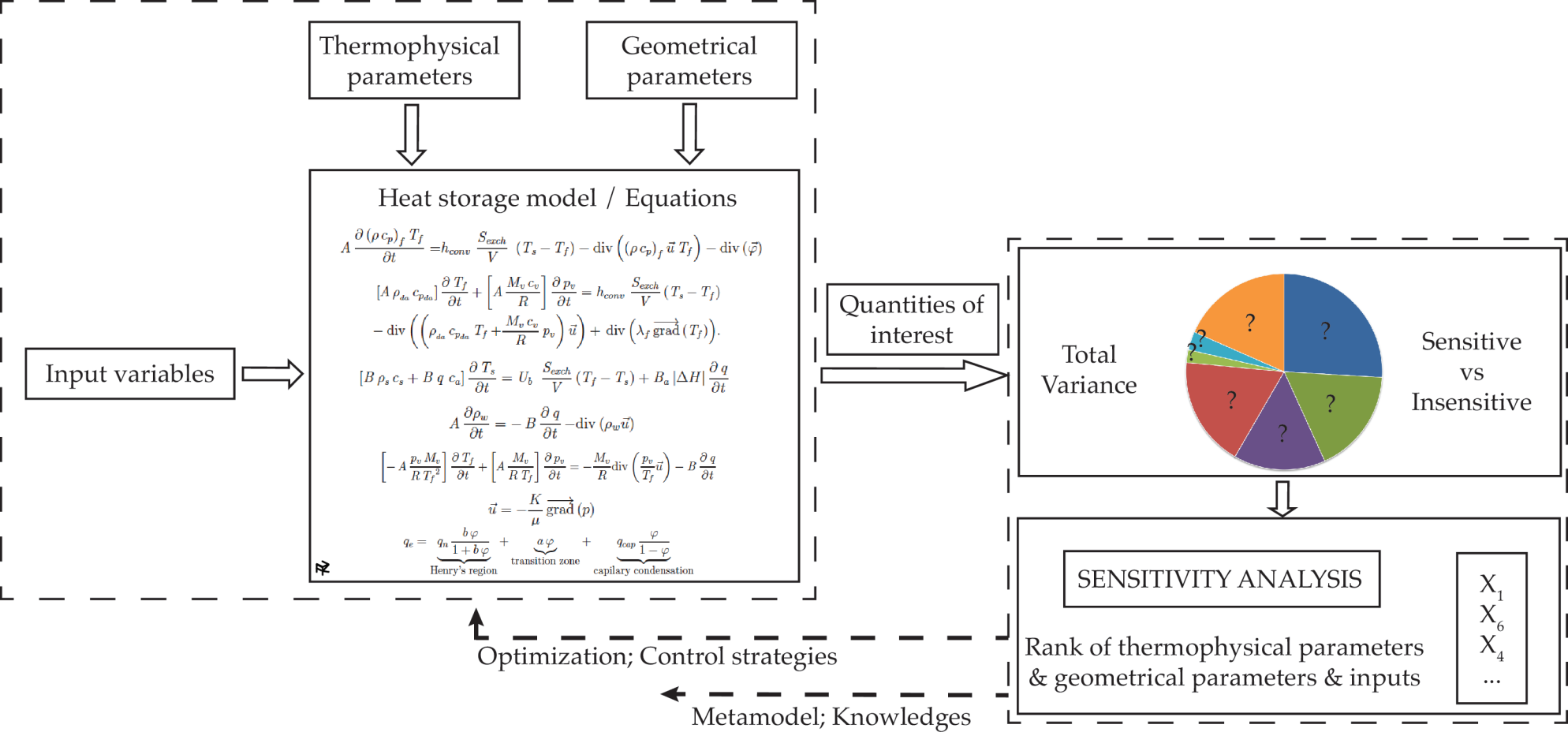
Thermophysical parameters
Geometrical parameters
Heat storage model / Equations
$A\frac{\partial(\rho c_p)_f T_f}{\partial t} = h_{conv}\frac{S_{exch}}{V}(T_s - T_f) - \mathrm{div}\left((\rho c_p)_f \vec{u} T_f\right) - \mathrm{div}(\vec{\varphi})$
$[A\rho_{da} c_{p_{da}}]\frac{\partial T_f}{\partial t} + \left[A\frac{M_v c_v}{R}\right]\frac{\partial p_v}{\partial t} = h_{conv}\frac{S_{exch}}{V}(T_s - T_f)$
$-\mathrm{div}\left(\left(\rho_{da} c_{p_{da}} T_f + \frac{M_v c_v}{R} p_v\right)\vec{u}\right) + \mathrm{div}\left(\lambda_f \overrightarrow{\mathrm{grad}}(T_f)\right).$
$[B\rho_s c_s + B q c_a]\frac{\partial T_s}{\partial t} = U_b \frac{S_{exch}}{V}(T_f - T_s) + B_a|\Delta H|\frac{\partial q}{\partial t}$
$A\frac{\partial \rho_w}{\partial t} = -B\frac{\partial q}{\partial t} - \mathrm{div}(\rho_w \vec{u})$
$\left[-A\frac{p_v M_v}{R T_f^2}\right]\frac{\partial T_f}{\partial t} + \left[A\frac{M_v}{R T_f}\right]\frac{\partial p_v}{\partial t} = -\frac{M_v}{R}\mathrm{div}\left(\frac{p_v}{T_f}\vec{u}\right) - B\frac{\partial q}{\partial t}$
$\vec{u} = -\frac{K}{\mu}\overrightarrow{\mathrm{grad}}(p)$
$q_e = \underbrace{q_n \frac{b\varphi}{1+b\varphi}}_{\text{Henry's region}} + \underbrace{a\varphi}_{\text{transition zone}} + \underbrace{q_{cap}\frac{\varphi}{1-\varphi}}_{\text{capilary condensation}}$
Input variables
Quantities of interest
Total Variance
Sensitive vs Insensitive
SENSITIVITY ANALYSIS
Rank of thermophysical parameters & geometrical parameters & inputs
X_1
X_6
X_4
...
Optimization; Control strategies
Metamodel; Knowledges